Assessment of performance enhancement of a semi-submersible vertical axis wind turbine with an optimized Darrieus rotor

Zhengshun Cheng[a,b], Kai Wang[c,*], Muk Chen Ong[d]

[a] *State Key Laboratory of Hydraulic Engineering Simulation and Safety, Tianjin University, Tianjin, China*
[b] *Department of Marine Technology and Centre for Autonomous Marine Operations and Systems, Norwegian University of Science and Technology, Trondheim, NO-7491, Norway*
[c] *Aker Solutions AS, 1366 Lysaker, Norway*
[d] *Department of Mechanical and Structural Engineering and Materials Science, University of Stavanger, Stavanger, NO-4036, Norway*

Abstract

Increasing efforts are currently being devoted to develop floating vertical axis wind turbines (VAWTs), due to their potential to reduce cost-of-energy. Optimization of rotors is favorable to increase the power capture and mitigate structural loads. In the DeepWind project, a baseline Darrieus type vertical axis wind turbine (VAWT) was first developed, followed by an optimized rotor. In this study, these two different rotors are adapted to a semi-submersible platform to achieve two floating VAWTs. The performance enhancement of the floating VAWT with the optimized rotor is evaluated by performance comparison with the floating VAWT with the baseline rotor. Numerical simulations are conducted using a fully coupled aero-hydro-servo-elastic simulation tool in time domain, under turbulent wind and irregular waves. Numerical analyses indicate that the floating VAWT with the optimized rotor greatly improves the performances with respect to power production, global platform motions, mooring line tensions, and especially tower base bending moments. The annual power production of the floating VAWT with the optimized rotor is improved by 11.3% as compared to that of the floating VAWT with the baseline rotor. However,

*Corresponding author.
Email address: zhengshun.cheng@gmail.com (Z. Cheng); wangkai.ntnu@gmail.com (K. Wang)

the variations of flapwise and edgewise bending moments along the blades are not improved for the optimized rotor, which might cause severe fatigue damage, and should be considered during the optimization of blades for VAWTs.
Keywords: floating vertical axis wind turbine, aero-hydro-servo-elastic, dynamic responses, optimized rotor, performance assessment

1. Introduction

The strong and stable wind at offshore locations and the increasing demand for energy have surged the application of wind turbines in deep water. Offshore wind power, the fastest growing source of renewable power generation in Europe, has attracted a lot of research institutes and companies to work on the development of floating wind turbines that ranges from conceptual proposals and numerical studies to development of methodologies and available simulations tools. Various concepts were developed and investigated by using different floating substructures to support different kinds of wind turbines. From the point of view of floating substructures, these concepts include the spar [1], the semi-submersible [2] and the tension leg platform (TLP) concepts [3]. Based on the wind turbine types, the floating wind turbines can be classified into floating horizontal axis wind turbines (HAWTs) and floating vertical axis wind turbines (VAWTs). Floating HAWTs have been widely studied and prototypes have been developed and tested, such as the Hywind demo in Norway, the WindFloat demo in Portugal and the floating wind turbines off the Fukushima coast of northeast Japan. Moreover, Hywind Scotland, which is the world's first floating wind farm, is being built by Statoil and is expected to start power production in late 2017.

Floating VAWTs are also a promising alternative in offshore wind energy because of their potential economic advantages. Compared with floating HAWTs, floating VAWTs have an ability to capture wind energy irrespective of wind direction without a yaw control mechanism, and lower centers of gravity. This could greatly reduce the cost-of-energy in application of large wind turbines

[4]. Moreover, floating substructures can help to mitigate the fatigue damages that are suffered by landbased VAWTs [5]. One more important merit is that floating VAWTs are more suitable for deploying as wind farms than floating HAWTs [6], since they are less affected by wake effects. The wake generated by a pair of counter-rotating H-rotors can dissipate more quickly than that of floating HAWTs, allowing them to be installed in wind farms with smaller separations. Thus, increasing efforts are devoted to the development of floating VAWTs, and various concepts of floating VAWTs have been evaluated, such as the DeepWind concept [7, 8] and the VertiWind concept [9], for conceptual designs and technical feasibility.

Several coupled simulation tools have been developed to investigate the response characteristics of floating VAWTs. An overview of capacities and differences of different simulation tools was summarized by Cheng et al. [10]. Based on developed simulation tools, studies have been performed with focus on the design, structural integrity, and dynamic responses so as to better understand the performance of the various concepts and further investigate the differences between floating HAWTs and floating VAWTs. The dynamic analysis and comparative studies of different floating VAWT concepts have been performed [11, 12, 13]. A novel concept that combines the 5 MW Darrieus curved blade VAWT with a semi-submersible platform has been extensively studied [5]. Additionally, a comparative study of three floating VAWT concepts (combinations of the 5 MW Darrieus curved bladed VAWT with a spar platform, with a TLP and with a semi-submersible, respectively) has been performed by Cheng et al. [14]. They concluded that the semi-submersible and the spar reduced the 2P effects on structural loads and mooring line tensions as compared to the TLP concept, at the expense of larger platform motions. The effect of blade number on the performance of VAWTs and dynamic behavior of floating straight-bladed VAWTs was comprehensively studied [15]. However, a more economically attractive and technically robust concept is still being developed.

The DeepWind concept [7] was proposed in the DeepWind project which was started in the autumn of 2010 under the European FP7 programme. It aimed at

investigating a new offshore floating vertical axis wind turbine (VAWT) concept for exploiting wind resources at deep offshore sites. It was firstly designed to be a 2 MW with the rotor height of 75 m and rotor diameter of 67 m [16], and was later increased to a larger size with power capacity of 5 MW as the first baseline design [7], followed by a further design optimization [8]. An optimized blade profile has been obtained with less weight and higher stiffness than the first baseline design [17]. Based on the optimized rotor, a new 5MW floating VAWT [18], which is composed of this optimized rotor and a semi-submersible, is studied by investigating dynamic motion and structural responses and compared with the baseline semi floating VAWT proposed by Wang et al. [19]. The results identified that the 5 MW optimized floating VAWT has lower fore-aft but higher lower side-side bending moments of structural components, lower motion amplitudes, lower short-term fatigue equivalent loads and a further reduced 2P effect [18]. However, the same controller is used for this comparison and the generated power above rated wind speed is much different for these two floating VAWTs. Therefore, optimized controllers are needed for both concepts.

In this study, optimized controllers are well designed for the baseline rotor and the optimized rotor, so that they have close power performance above the rated wind speed. For these two floating VAWTs, numerical simulations are conducted using a fully coupled aero-hydro-servo-elastic simulation tool in time domain, under turbulent wind and irregular waves. The performance enhancement of the floating VAWT with the optimized rotor is evaluated by comparing with the floating VAWT with the baseline rotor in terms of power performance, platform motions, structural loads and mooring line tensions.

2. Floating wind turbine model

2.1. Description of baseline and optimized rotors

The DeepWind project is an European Union (EU) project that aims for better cost of energy and a more reliable wind turbine. During the DeepWind project, two Darrieus rotors were developed, including a baseline rotor [7] and a

optimized rotor [8, 20]. In this study, both the baseline and optimized rotors are considered, and the performance enhancement of the optimized rotor is assessed by a comparison with the baseline rotor.

Fig. 1 depicts the sketches of the baseline and optimized rotors. Main specification of these two rotors are given in Table 1. These two rotors have the same rated power, and identical cut-in, rated, and cut-out wind speeds. However, the geometry of these two rotors are quite different. Compared to the baseline rotor, the optimized rotor has increased blade length and blade height, and reduced rotor diameter and blade chord length. As a result, the optimized rotor has a smaller solidity than that of the baseline rotor. The blades of the optimized rotor are made of pultruded glass fiber reinforced epoxy, while the blades of the baseline rotor is made of pultruded glass fiber reinforced plastics. The rated rotational speed of the optimized rotor is also higher than that of the baseline rotor. Additionally, the tower supporting the rotor is also optimized for the optimized rotor.

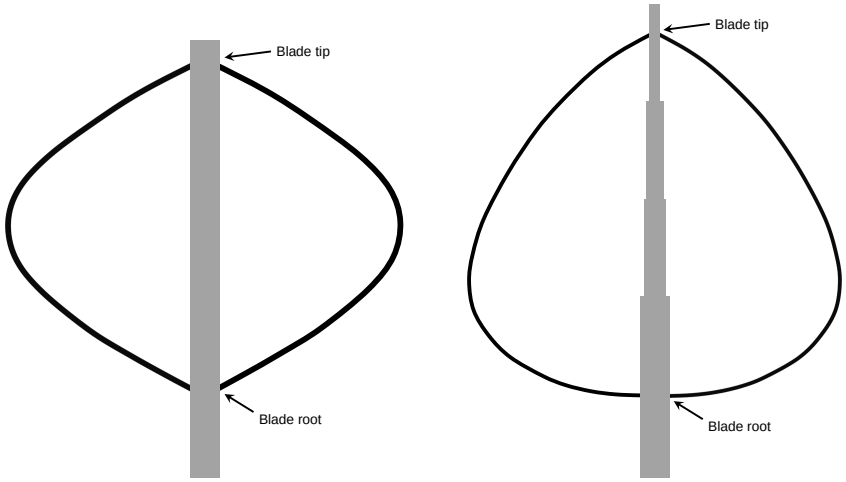

(a) The baseline rotor (b) The optimized rotor

Figure 1: Sketches of two rotors. (a) the baseline rotor (b) the optimized rotor.

Table 1: Main specifications of the baseline and optimized rotors

	Baseline rotor	Optimized rotor
Rated power [MW]	5	5
Rated rotational speed [rpm]	5.26	5.95
Number of blades N	2	2
Rotor radius R [m]	63.74	60.48
Rotor height H [m]	129.56	143
Blade length [m]	188.86	200.4
Blade chord length c [m]	7.45	5
Solidity $\sigma = \frac{Nc}{R}$	0.234	0.165
Airfoil type	NACA0018	NACA0018
Cut-in, rated, cut-out wind speed [m/s]	5, 14, 25	5, 14, 25
Rotor mass [ton]	757.76	450.76
Center of mass [m]	(0, 0, 75.38)	(0, 0, 75.82)

It should be noted that the main specifications of the optimized rotor are slightly different from the original design in terms of airfoil type. In the original design of the optimized rotor, the airfoil NACA0025 is applied at two ends of each blade, including a section with a length of 21.7 m close to the upper end and 29.44 m close to the lower end. The use of NACA0025 is to increase the strength of the blades at two ends, which suffer considerable loads and are likely to fail during the operation. However, during the numerical simulation in this study, these sections with NACA0025 airfoils are replaced with NACA0018 airfoils, due to the limitation of the current simulation tool. Such modification will not significantly change the aerodynamic performance of the optimized rotor, since these sections with NACA0025 airfoil are located close to blade ends that are connected to the tower, and their contribution to total aerodynamic loads are very limited.

2.2. Description of floating VAWTs

Both the baseline and optimized rotors are adapted to a semi-submersible platform to achieve two floating VAWTs, as illustrated in Fig. 2. The semi-submersible considered is from the DeepCwind phase II of the OC4 project

[21], which was originally designed for the NREL 5MW horizontal axis wind turbine [22] in a water depth of 200 m. This semi-submersible was later modified by Wang et al. [19] to support the baseline rotor described above. The basic principle for the modification was that the draft and displacement of the floater held the same, while the ballast in the platform was adjusted to counteract the change in the mass of the rotor. In this study, the same principle was employed to adjust the semi-submersible for the optimized rotor. Since the difference in rotor mass between the NREL 5MW wind turbine and the baseline and optimized rotors considered in this study is very small compared to the displacement of the platform, it is thus assumed that such modification will not change significantly the hydrostatic performance of the floating system. More detailed information about the semi-submersible and how to adjust the ballast are described by Robertson et al. [21] and Cheng et al. [14], respectively.

Main properties of the floating VAWT systems with the baseline and optimized rotors are given in Table 2. The generator is assumed to be placed at the tower bottom. Due to the adjustment of ballast, the platform masses (including ballast and generator masses) of these two floating VAWTs presents small difference, so does the center of mass of the platforms. Consequently, the hydrostatic restoring coefficients in heave, roll and pitch motions, are slightly different. The moment of inertia in yaw between these floating VAWT systems are also fairly close, but the moments of inertia in pitch and roll are not. This is because the baseline and optimized rotors are located more than 80 m above the mean water level, the moment of inertia of the optimized rotor will be much smaller than that of the baseline rotor due to less mass of the optimized rotor. As a result, the total moment of inertia in pitch and roll differs between these two floating VAWT systems. This is also observed in the natural periods of rigid-body motions for these two floating VAWT systems, which are numerically estimated by conducting free decay tests. The natural periods in surge, sway, heave and yaw between these two floating VAWTs are very close to each other, while those in pitch and roll present much differences. These differences are mainly due to the different moments of inertia in roll and pitch.

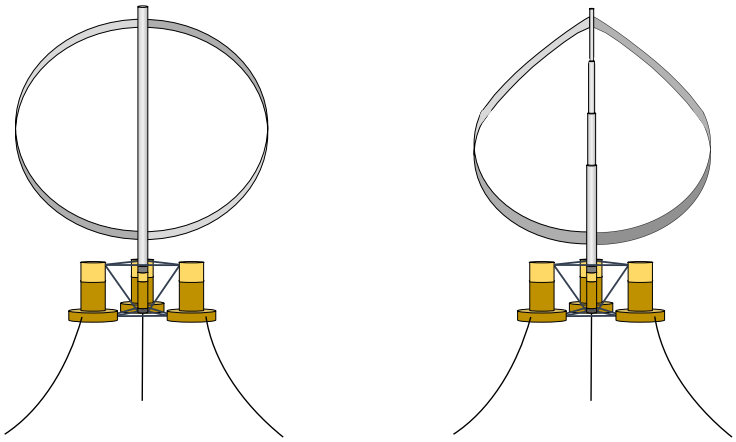

(a) Floating VAWT with the baseline rotor

(b) Floating VAWT with the optimized rotor

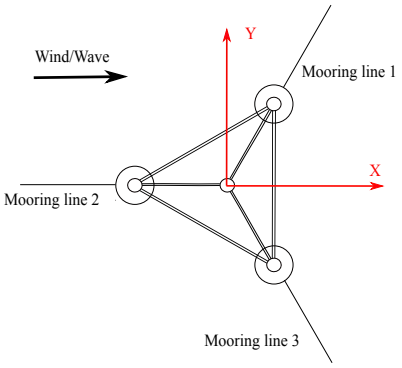

(c) Mooring system

Figure 2: Numerical models of floating VAWT systems. (a) floating VAWT with the baseline rotor, (b) floating VAWT with the optimized rotor. (c) mooring system

The global coordinate system is defined as shown in Fig. 2c. The origin is located at the center of the waterplane of the platform, and Z is positive upwards. The directions of X and Y are illustrated in Fig. 2c. In addition, it is assumed in this study that the wind and waves considered later come from the negative X direction.

Table 2: Properties of the floating VAWT systems with the baseline and optimized rotors

	Floating VAWT with the baseline rotor	Floating VAWT with the optimized rotor
Water depth [m]	200	200
Draft [m]	20	20
Diameter of side and center columns at mean water level [m]	12.0/6.5	12.0/6.5
Platform mass, including ballast and generator [ton]	13353.7	13614
Center of mass for platform [m]	(0, 0, -13.42)	(0, 0, -13.98)
Buoyancy in undisplaced position [kN]	139816	139816
Center of buoyancy [m]	(0, 0, -13.15)	(0, 0, -13.15)
Surge/Sway natural period [s]	114.0	113.1
Heave natural period [s]	17.1	17.1
Roll/Pitch natural period [s]	31.0	20.7
Yaw natural period [s]	79.7	80.4

3. Methodology

3.1. Fully coupled numerical method

The fully coupled aero-hydro-servo-elastic code, namely SIMO-RIFLEX-AC [23] is used for numerical modeling and dynamic analysis of floating VAWTs in time domain in the present study. The SIMO-RIFLEX-AC code is able to account for the turbulent wind inflow, aerodynamics, hydrodynamics, structural dynamics, control system dynamics and mooring line dynamics. It has been verified by a series of numerical comparisons with the codes HAWC2 and SIMO-RIFLEX-DMS [23]. Three computer codes are integrated in the SIMO-RIFLEX-AC code, including SIMO[24], RIFLEX[25] and AC. The SIMO and RIFLEX codes were developed by SINTEF OCEAN (formerly MARINTEK) and have been widely used in the offshore oil and gas, and wind turbine industries.

The hydrodynamic loads acting on the semi-submersible is modeled in SIMO through a combination of potential flow theory and Morison's equation. Hydrodynamic coefficients, such as added masses, potential dampings, transfer functions of wave excitation forces, are first estimated in frequency domain by a potential flow solver and then applied in time domain using the convolution technique [26]. Viscous drag forces on the platform hull is included using the Morison's formula. Morison's formula is also applied to the brace and mooring lines that are not included in the potential flow model.

The aerodynamic loads acting on blades are estimated using the AC code

[27]. The AC code was developed based on the actuator cylinder flow theory, originally proposed by Madsen [28] and further improved by Cheng et al. [27]. It can provide a higher accuracy than the double multi-stream tube method at a small computational cost [29]. In the AC code, effects of wind shear and turbulence, dynamic inflow and dynamic stall are all considered. However, the effect of tower shadow is neglected.

The structural dynamics of the floating wind turbine system is modeled using RIFLEX. The semi-submersible including the braces is represented as a rigid body; the blades, tower and shaft are modeled using nonlinear beam elements; and the mooring lines are considered as nonlinear bar elements. A very short tower close to the tower base is used to connect the rotating shaft and semi-submersible through a flexible joint. Structural properties of the blades, tower and shaft of the baseline and optimized rotors are respectively described in [30] and [31], and are thus not presented in this paper. RIFLEX provides interfaces with SIMO and AC respectively so that hydrodynamics and aerodynamics are coupled with structural dynamics. Additionally, RIFLEX also provides a link to an external controller, in which a generator torque is applied through the flexible joint to regulate the rotor rotational speed. The generator torque is adjusted by a controller based on the proportional-integral (PI) control algorithm. More details about the control strategy applied in the study is described in the next section.

3.2. Control strategy

In this study, the control strategy proposed by Cheng et al. [12] is adopted. It is a PI-based generator torque controller that can enable variable-speed and fixed-pitch operation for a VAWT. During the numerical simulation, the measured rotational speed was filtered through a low-pass filter. The controller aims to minimize the error between the measured and filtered rotational speed Ω_{mes} and the reference rotational speed Ω_{ref},

$$\Delta\Omega = \Omega_{mes} - \Omega_{ref} \tag{1}$$

in which the reference rotational speed Ω_{ref} is defined as illustrated in Fig. 3. The rotational speed error $\Delta\Omega$ is then fed through the proportional and integral paths to obtain an updated value of the required electric torque, as follows,

$$T(t) = K_G \left(K_P \Delta\Omega(t) + K_I \int_0^t \Delta\Omega(\tau) d\tau \right) \tag{2}$$

in which K_G is the generator stiffness, and K_P and K_I are the proportional and integral gains, respectively.

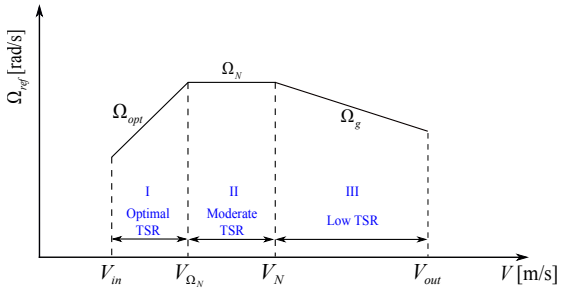

Figure 3: The relationship between the reference rotor rotational speed and the wind speed for the controller considered. V_{in}, V_N and V_{out} are the cut-in, rated, and cut-out wind speed, respectively; V_{Ω_N} is the wind speed for the rated rotational speed; Ω_N is the rated rotational speed; Ω_{opt} is the optimal rotational speed that can maximize the power capture; Ω_g is the rotational speed that can hold the mean generator power approximately constant. (reproduced from Cheng et al. [23])

During the implementation, the reference rotational speed is obtained using a look-up table based on the measured and filtered rotational speed and the filtered generator torque. Details about the implementation are described in Cheng et al. [23].

By employing this control strategy, the generator power performance of these two floating VAWTs were simulated, as shown in Fig. 4. The generator power shown here is the mean value under steady wind conditions. We can see that the mean generator power above the rated wind speed is approximately constant for each floating VAWT, and they are fairly close. While below the rated wind speed, the floating VAWT with the optimized rotor gives larger mean generator power, indicating that it has a better power performance than the

floating VAWT with the baseline rotor. The mean values of rotor rotational speeds under different wind speeds are also presented in Fig. 4b. The floating VAWT with the optimized rotor operates at a higher rotational speed than the floating VAWT with the baseline rotor. It should be noted that these mean rotational speed shown in Fig. 4b indicates the frequency per revolution (i.e. 1P frequency) under different wind speeds for each floating VAWT, which will be used later when analyzing the responses due to periodic aerodynamic loads.

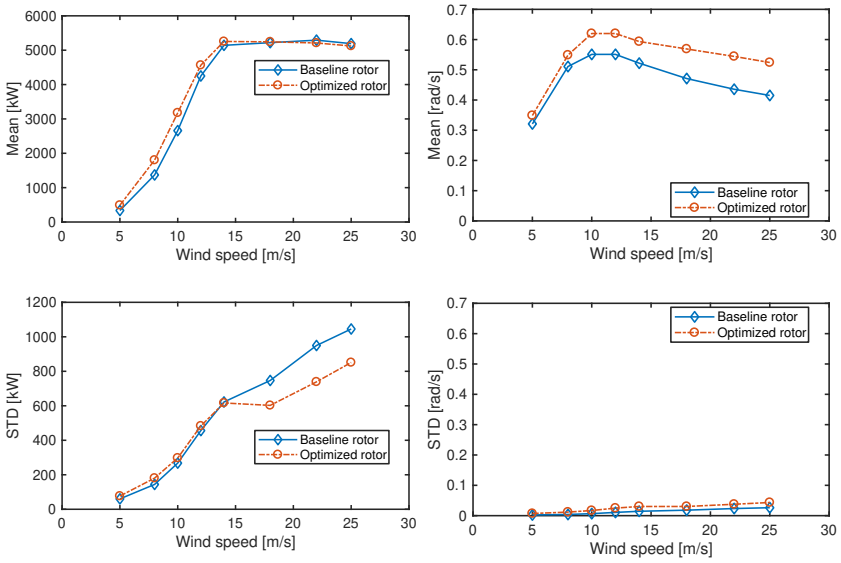

(a) Generator power (b) Rotor rotational speed

Figure 4: The steady-state performance of the floating VAWTs with the baseline and optimized rotors. (a) Generator power (b) rotor rotational speed.

4. Environmental conditions and load cases

To evaluate the performance of these two floating VAWT concepts, a realistic environmental condition should be considered. In this paper, the wind and wave data at the Statfjord site in the northern North Sea is selected. A set of environmental conditions is selected to simulate the dynamic responses of these two floating VAWTs, as given in Table 3. In this paper, only normal operating

conditions with the wind speed ranging from the cut-in to cut-out are considered. The turbulent wind and irregular waves are correlated and directionally aligned.

Table 3: Load Cases –combined wind and waves

	U_w [m/s]	T_I	H_s [m]	T_p [s]	Simulation length [s]
LC1	5	0.224	2.10	9.74	3600
LC2	8	0.174	2.55	9.86	3600
LC3	10	0.157	2.88	9.98	3600
LC4	12	0.146	3.24	10.12	3600
LC5	14	0.138	3.62	10.29	3600
LC6	18	0.127	4.44	10.66	3600
LC7	22	0.121	5.32	11.06	3600
LC8	25	0.117	6.02	11.38	3600

U_W: mean wind speed at refernce height; T_I: turbulence intensity; H_S: significant wave height; T_P: peak period

The 3D turbulent wind field is generated in TurbSim [32] based on the Kaimal spectral model, which is defined in IEC 61400 [33]. In addition, the wind shear is considered using the normal wind profile model proposed in the IEC 61400 [33].

$$U(z) = U_{ref}\left(\frac{z}{z_{ref}}\right)^{\alpha} \tag{3}$$

where U_{ref} is the reference wind speed, z_{ref} is the height of the reference wind speed and α is the power law exponent. In this study z_{ref} is set to be 79.78 m above mean sea level, which is the vertical center of blades of the baseline rotor considered. The reference height for the optimized rotor is about 86.5m, but this value is not used to create the wind field because applying identical wind field for these two rotors is favorable for the performance assessment. The value of α is chosen to be 0.14 for the floating wind turbines according to IEC 61400-3 [33]. Regarding irregular wave conditions, long-crested irregular waves are generated using the Joint North Sea Wave Project (JONSWAP) spectrum.

In this study, the same wind and wave fields are applied for these two floating

VAWTs. For each LC, 5 identical and independent simulations with different random seed numbers are carried out, which is used to reduced the stochastic variation of dynamic responses.

5. Results and discussion

5.1. Annual power production performance

The optimized rotor improves the power production performance of the floating wind turbine system. In this section the characteristics of power production and annual power production performance of the floating VAWTs are assessed.

Fig. 5 represents the mean value and standard deviation of the generator power for the floating VAWTs with baseline and optimized rotors. The wind considered is turbulent and the waves are irregular. Compared to the steady state results of generator power shown in Fig. 4a, the mean values of the generator power in Fig. 5 follow similar trend as those in Fig. 4a. This indicates that the control strategies implemented in this study work well in both steady and turbulent wind conditions. Additionally, the standard deviations of the generator power in Fig. 5 are generally larger than those in Fig. 4a. This is mainly due to the turbulent wind, which causes low-frequency variation of the generator power.

The mean values and standard deviations of the generator power are also compared to those estimated by Ishie et. al [18]. Ishie et. al [18] conducted similar simulations to investigate the structural dynamic responses of these floating VAWTs. However, for the numerical simulations by Ishie et. al [18], the controllers were not sufficient for the baseline and optimized rotors. The controllers were not able to control the power production above the rated wind speed. As a result, the mean generator power above the rated wind speed deviated significantly from each other, as shown in Fig. 5a. In this study, the controller are newly designed for the baseline and optimized rotors, which approximately makes the mean generator power between these two rotors fairly close. Hence,

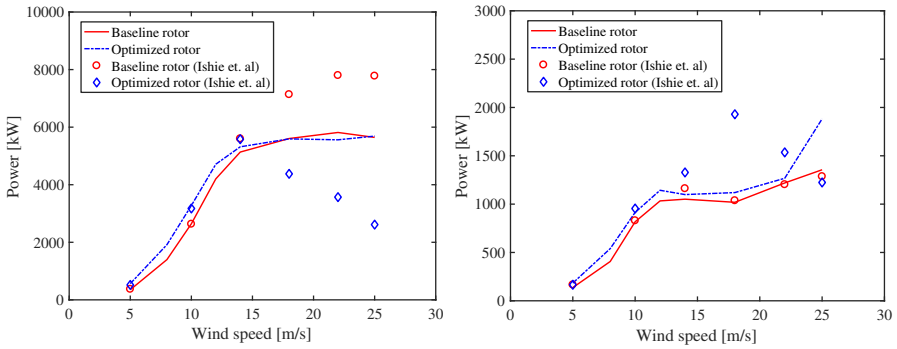

(a) Mean value (b) Standard deviation

Figure 5: The mean value and standard deviation of generator power production for floating VAWTs with baseline and optimized rotors under turbulent wind and irregular waves. The results are compared to those estimated by Ishie et. al [18]

evaluating the performance enhancement of the floating VAWT due to the optimized rotor is more reasonable, compared to those by Ishie et. al [18].

Given the distribution of mean wind speed and the power performance of the turbine, the annual power production performance of a floating wind turbine can be roughly estimated. The availability of these turbines is assumed to be 1. According the study by [34], the marginal distribution of mean wind speed at the site considered at 10 m above the MSL can be described by a 2-parameter Weibull distribution :

$$F(U_W) = 1 - exp\left(-\left(\frac{u_w}{\beta}\right)^{\alpha}\right) \tag{4}$$

where α and β are the shape and scale parameters, respectively, and they were determined to be $\alpha = 1.708$ and $\beta = 8.426$ based on the measurements from the Northern North Sea in the period 1973-99. Since the wind speed at the reference height of 79.78m can be estimated based on the wind speed at 10 m according to Eq. 3, the corresponding probability density function of the mean wind speed at the reference height of 79.78m can be computed, as demonstrated in Figure 6. It is worth noting here that the reference heights for the baseline rotor and for the optimized rotor are different, but the time domain simulations are conducted under the same wind field, which is created assuming a reference

height of 79.78m. Therefore, the distribution of mean wind speed shown in Figure 6 is applicable for both the baseline rotor and the optimized rotor.

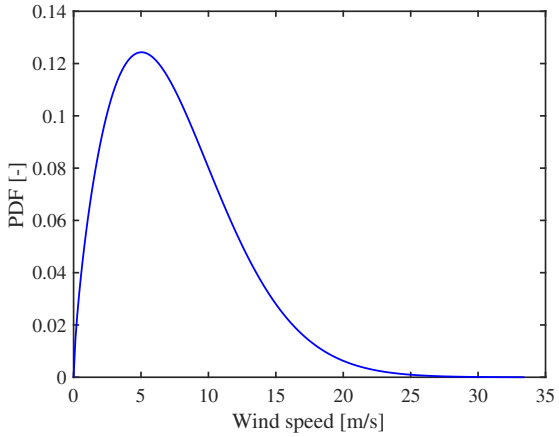

Figure 6: The probability density function (PDF) of the mean wind speed at the reference height of 79.78m.

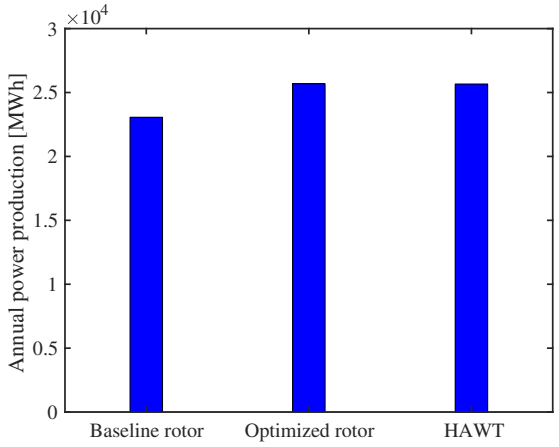

Figure 7: The estimated annual power production for the floating HAWT and VAWTs.

The estimated annual power production for the baseline rotor and the optimized rotor, as plotted in Fig. 7, are about 23.0 GWh and 25.6 GWh, respectively. The enhancement of annual power production of the optimized rotor is approximately 11.3%. In addition, as estimated by [13], the annual power production of the similar semi-submersible platform supporting the NREL 5MW

HAWT is also about 25.6 GWh. This implies that the floating VAWT with the optimized rotor can produce more or less the same power as the floating horizontal axis wind turbine.

5.2. Characteristics of aerodynamic loads

Fig. 8 presents the mean values and standard deviations of thrust and lateral force of the floating VAWTs with the baseline and optimized rotors. It can be found that below the rated wind speed (14 m/s), the mean value and standard deviation of the thrusts of the baseline and optimized rotors are very close to each other, while above the rated wind speed, the mean value and standard deviation of the thrust of the optimized rotor are both smaller than those of the baseline rotor. Regarding the lateral force, the standard deviations of the baseline and optimized rotors are almost the same, and the mean value of the optimized rotor is smaller than that of the baseline rotor. Despite its better power performance, the optimized rotor is subjected to relatively smaller aerodynamic loads than the baseline rotor under the same wind condition.

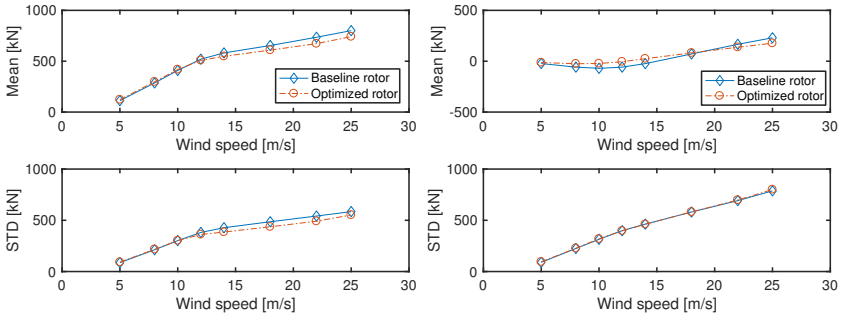

(a) Thrust (b) Lateral force

Figure 8: The mean values and standard deviations of (a) thrust and (b) lateral force of the floating VAWTs with the baseline and optimized rotors under turbulent wind and irregular waves.

5.3. Characteristics of platform motions

The platform motion characteristics of the floating VAWTs are demonstrated in Fig. 9. It can be observed in Fig. 9 that the floating VAWT with the optimized

rotor has relatively smaller absolute mean value in motions of surge, sway, roll, pitch and yaw than the floating VAWT with the baseline rotor. So does the standard deviation, except for the surge motion. The floating VAWT with the optimized rotor has relatively larger standard deviation in surge motion for wind speed above 14 m/s. Since the wave condition applied on these two floating VAWTs are identical, wave induced responses are likely to be fairly close, and consequently, discrepancies in terms of platform motions may be due to wind-induced responses, i.e. because of the difference in rotors. This phenomenon is demonstrated by power spectral analyses.

Fig. 10 shows the power spectra of surge, sway, roll and yaw motions of the floating VAWTs under LC7. Regarding the surge spectrum, the wave frequency responses between these two floating VAWTs are identical, but the low frequency responses differ significantly. These low frequency responses are surge resonant responses, which are induced by low frequency turbulent wind. The sway and yaw spectra of these two floating VAWTs also differ in the low frequency responses, which are respectively the sway and yaw resonant responses due to turbulent wind as well.

Power spectra of pitch motions of the two floating VAWTs under LC3 and LC7 are shown in Fig. 11. Unlike the spectra of surge and yaw motions, notable differences are observed in the pitch spectra in a wide range of frequencies between these two floating VAWTs. Compared to the floating VAWT with the optimized rotor, the floating VAWT with the baseline rotor has relatively larger low-frequency responses and pitch resonant responses, which are both due to low frequency turbulent winds. Nevertheless, the floating VAWT with the optimized rotor has slightly larger wave frequency responses. Additionally, responses corresponding to the 2P frequencies are both observed in the pitch spectrum. The 2P frequencies for the floating VAWTs with the baseline rotor and with the optimized rotor are 1.1 rad/s and 1.24 rad/s under LC3, and 0.86 rad/s and 1.08 rad/s under LC7, respectively. The floating VAWT with the baseline rotor has a much larger 2P responses than the floating VAWT with the optimized rotor, which implies that the 2P response in pitch motion can

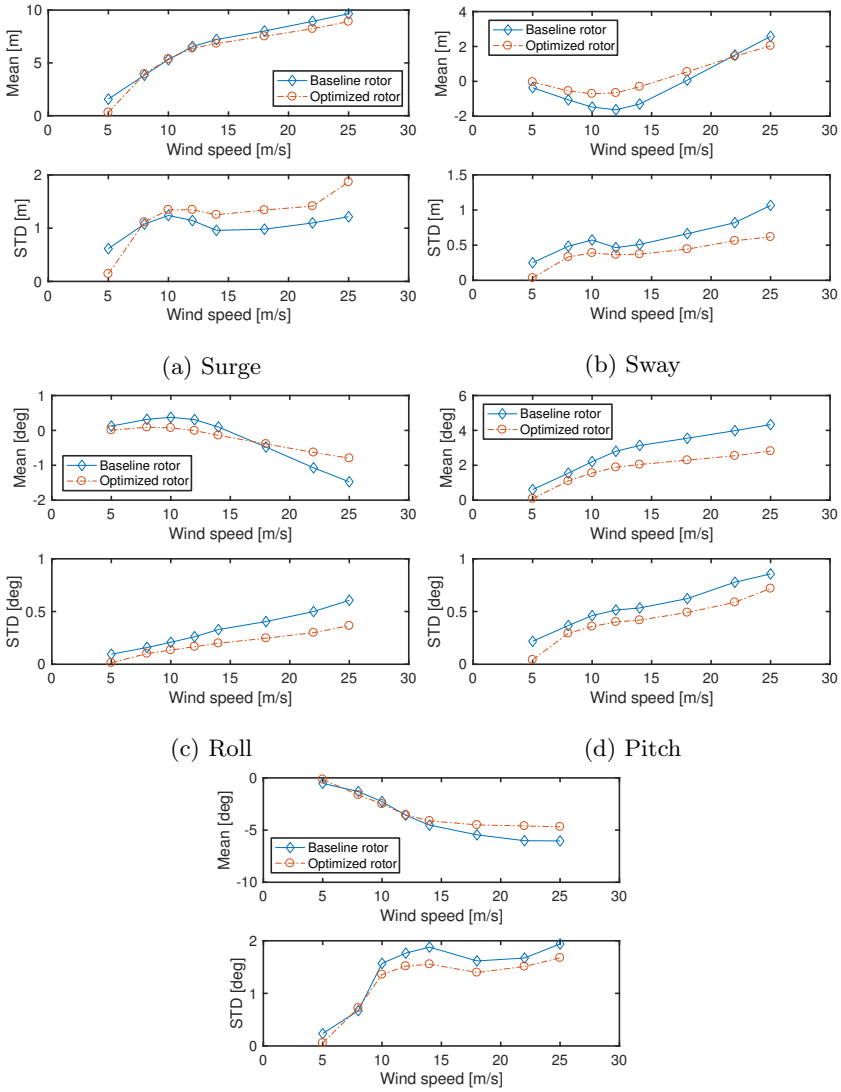

(a) Surge

(b) Sway

(c) Roll

(d) Pitch

(e) Yaw

Figure 9: Mean values and standard deviations of platform motions of the baseline and optimized floating vertical axis wind turbines (VAWTs) under turbulent wind and irregular waves. (a) Surge (b) Sway (c) Roll (d) Pitch (e) Yaw.

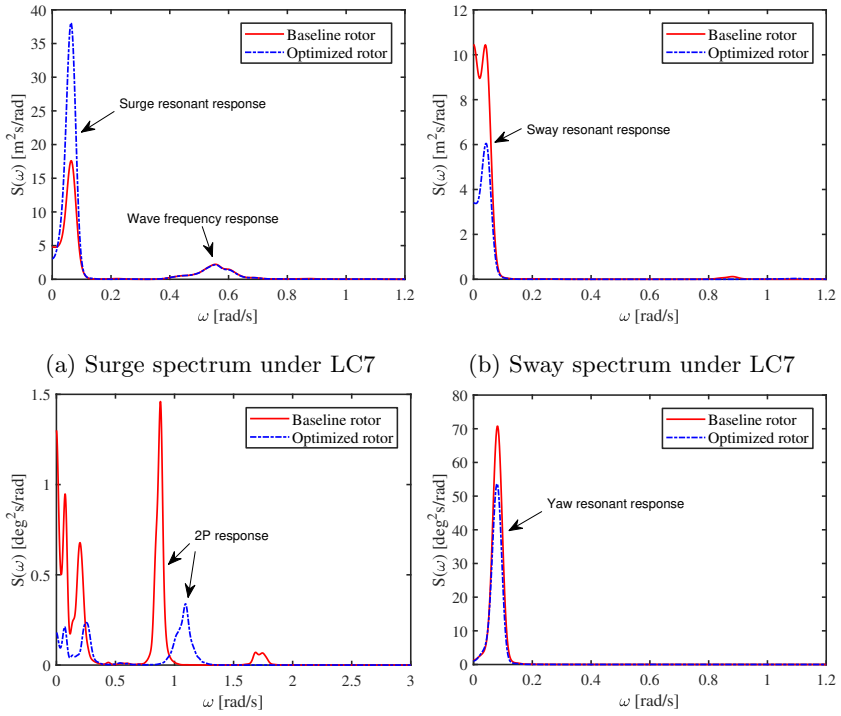

(a) Surge spectrum under LC7 (b) Sway spectrum under LC7

(c) Roll spectrum under LC7 (d) Yaw spectrum under LC7

Figure 10: Power spectra of surge, sway, roll and yaw motions of the floating VAWTs with the baseline and optimized rotors under LC7.

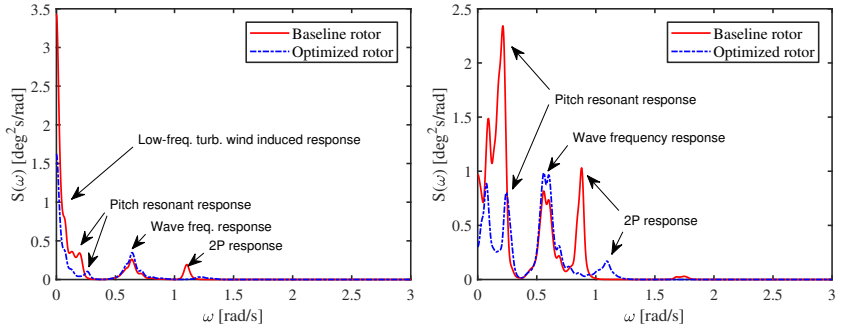

(a) Pitch spectrum under LC3 (b) Pitch spectrum under LC7

Figure 11: Power spectra of pitch motion of the floating VAWTs with the baseline and optimized rotors under LC3 and LC7.

be mitigated by adopting the optimized rotor. Moreover, the difference in the pitch responses are mainly due to the overturning moments caused by the thrust force. The blade shape is optimized for the optimized rotor to achieve a small overturning arm. As a result, the wind induced pitch moment is smaller for the optimized rotor, even though the thrust forces of these two rotors are fairly close.

Similar observations are found in the roll spectrum, as shown in Fig. 10c. The roll responses are dominated by the low frequency turbulent wind induced responses and 2P responses. It appears that the floating VAWT with the optimized rotor gives smaller responses with respect to the low frequency responses and 2P responses than the floating VAWT with the baseline rotor.

5.4. Characteristics of tower base bending moments

Previous studies [14, 13] shows that the floating VAWTs have extremely severe fatigue issue at the tower base. Hence the tower base bending moments of these two floating VAWTs are studied to assess whether the optimized rotor can help to mitigate the fatigue damage at the tower base.

Fig. 12 presents the mean values and standard deviations of tower base bending moments of the floating VAWTs. Both tower base fore-aft bending moment and side-side bending moment are considered here. In general, the floating VAWT with the optimized rotor gives smaller mean values and standard deviations of the tower base fore-aft and side-side bending moments than the floating VAWT with the baseline rotor. These differences between these two floating VAWTs increase as the mean wind speed in each case increases. Using the optimized rotor can reduce the mean values and standard deviations of the tower base fore-aft bending moment up to 30% and 36%, respectively. This is a considerable large reduction, and can in turn extend the fatigue life for the tower significantly.

As indicated in previous study [14], the tower base bending moments are contributed from the aerodynamic loads acting on the rotor and the self weight of the rotor when a floating VAWT system is tilt. Regarding the bending moments

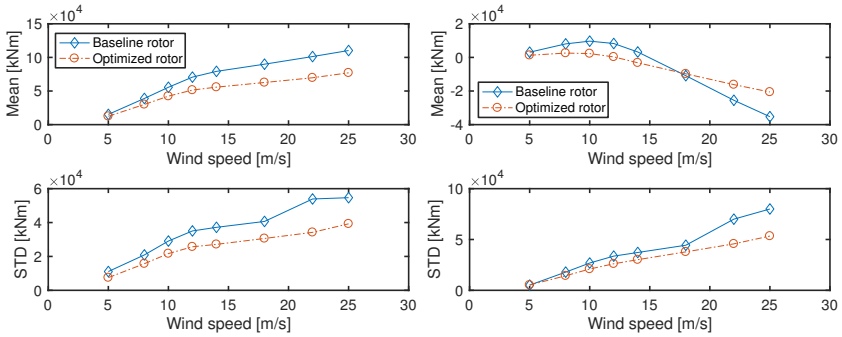

(a) Fore-aft bending moment (b) Side-side bending moment

Figure 12: Mean values and standard deviations of tower base (a) fore-aft (b) side-side bending moments of floating VAWTs with the baseline and optimized rotors under turbulent wind and irregular waves.

caused by aerodynamic loads, the optimized rotor has a shorter overturning arm with respect to the tower base than the baseline rotor. Consequently, the tower base bending moments due to aerodynamic loads are smaller for the floating VAWT with the optimized rotor as compared to the floating VAWT with the baseline rotor. In addition, the floating VAWT with the optimized rotor has a smaller pitch motion than the floating VAWT with the baseline rotor, which can subsequently reduce the bending moments caused by the self weight of the rotor.

Power spectra of the tower base bending moments are also analyzed for two representative LCs, i.e. LC3 and LC7, as shown in Figs. 13 and 14. It can be clearly observed that the tower base fore-aft bending moment and side-side bending moment are both dominated by the 2P response, which is due to the periodic aerodynamic loads. The floating VAWT with the optimized rotor has a much smaller 2P response than the floating VAWT with the baseline rotor. In addition, the floating VAWT with the baseline rotor also presents responses in the vicinity of 1.68 rad/s, especially at high wind speed (see Fig. 14). The possible reason is that resonant structural responses of the baseline rotor are excited. Natural frequencies of the baseline rotor was investigated by [19]. The

natural frequency of 1st blade flatwise modes is located at 1.68 rad/s.

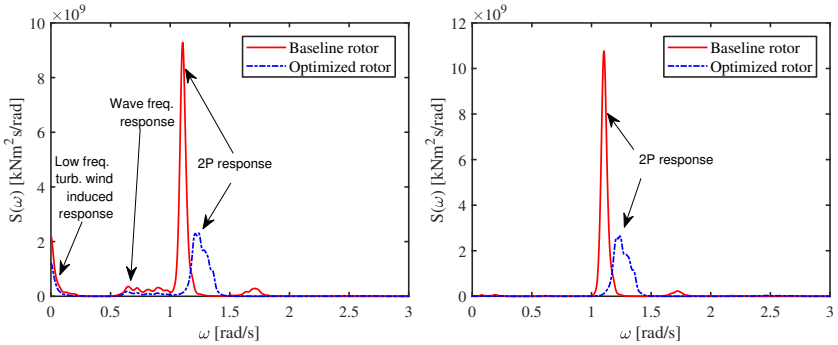

(a) Fore-aft bending moment (b) Side-side bending moment

Figure 13: Power spectra of tower base (a) fore-aft bending moment and (b) side-side bending moment of the floating VAWTs with the baseline and optimized rotors under LC3.

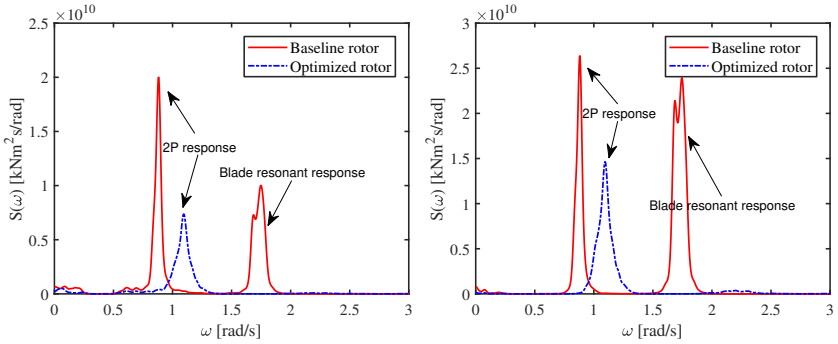

(a) Fore-aft bending moment (b) Side-side bending moment

Figure 14: Power spectra of tower base (a) fore-aft bending moment and (b) side-side bending moment of the floating VAWTs with the baseline and optimized rotors under LC7.

5.5. Characteristics of blade loads

The structural load responses along the blades are also investigated in the present study. Here four representative load cases are considered, i.e. LC1 with mean wind speed of 5 m/s, LC3 with mean wind speed of 10 m/s, LC5 with mean wind speed of 14 m/s, and LC8 with mean wind speed of 25 m/s. Fig. 15

presents the distribution of mean values and standard deviations of structural loads along the blade for these two floating VAWTs, including the axial force, the flapwise bending moment and the edgewise bending moment.

In Fig. 15, the dimensionless blade length at 0 indicates the blade root, and that at 1 represents the blade tip. It can be clearly found that the optimized rotor reduces the mean values of axial force along the blade, especially at the upper part of the blade. However, the standard deviation of the axial force at the lower part of the blade is greatly increased for the optimized rotor compared to the baseline rotor. At the upper part of the blade, the standard deviations of the axial force between the optimized rotor and the baseline rotor are fairly close.

The optimized rotor has a close to zero flapwise bending moment at the blade root, which is reduced significantly compared to the baseline rotor. The variation of flapwise bending moment along the blade of the optimized rotor differs significantly from that of the baseline rotor. At the blade tip, both the baseline and optimized rotors have very large flapwise bending moment, but with different bending direction.

The mean values of the edgewise bending moment along the blade between these two rotors also differ with each other. However, the mean values of the edgewise bending moments are relatively small compared to those of the flapwise bending moments, for both the baseline and optimized rotors.

For the standard deviations of the flapwise and edgewise bending moments, the optimized rotor gives considerably larger responses along the blade than the baseline rotor, especially at high wind speeds. Power spectral analyses are carried out for the flapwise and edgewise bending moments of the blade. Fig. 16 shows the power spectra of the flapwise and edgewise bending moments at the mid of the blade under LC3. The power spectral responses of the baseline rotor, including both the flapwise and edgewise bending moments, are several order of magnitude smaller than those of the optimized rotor. For the optimized rotor, both the flapwise and edgewise bending moments are dominated by notable 1P responses and by a relatively small 2P response. While for the baseline rotor,

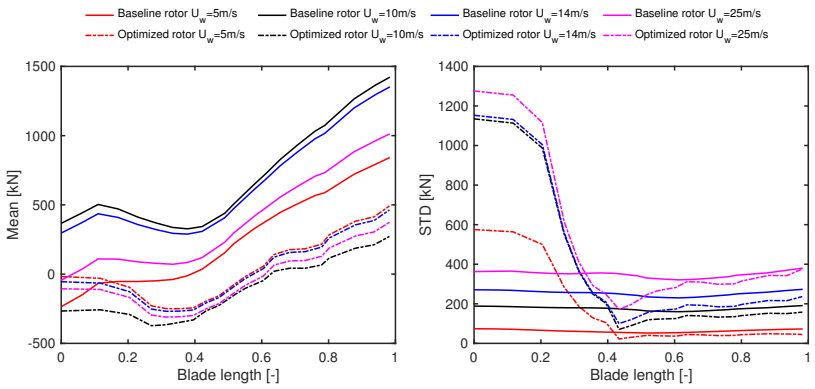

(a) Axial force

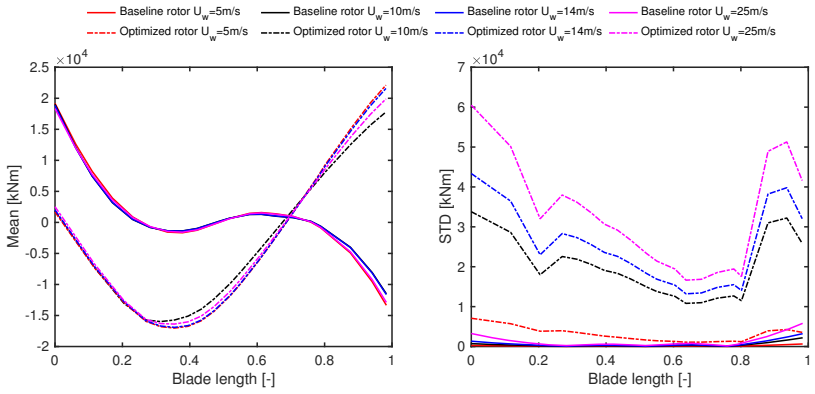

(b) Flapwise bending moment

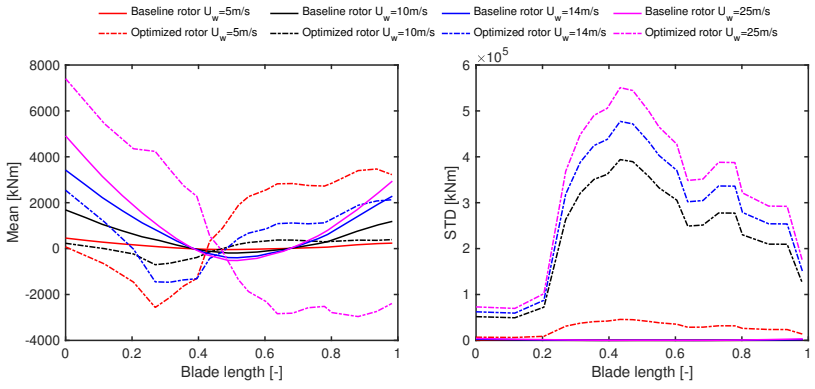

(c) Edgewise bending moment

Figure 15: Mean values and standard deviations of structural responses along blade of the floating VAWTs with the baseline and optimized rotors in turbulent wind and irregular waves. Here U_w in the legend denotes the mean wind speed.

the 1P response is extremely dominating for both the flapwise and edgewise bending moments, and a small 2P response is observed in the flapwise bending moment and small 3P and 5P responses are observed in the edgewise bending moment.

It should be noted that as mentioned in section 2.1, the optimized rotor considered in this study is modified on the basis of the original design, in terms of the airfoil type. The airfoil NACA0025 is applied at two ends of the blade, which implies that the structures at two ends of the blade will be stronger, and the overall structural load performance of the blade will be better than that of the baseline rotor.

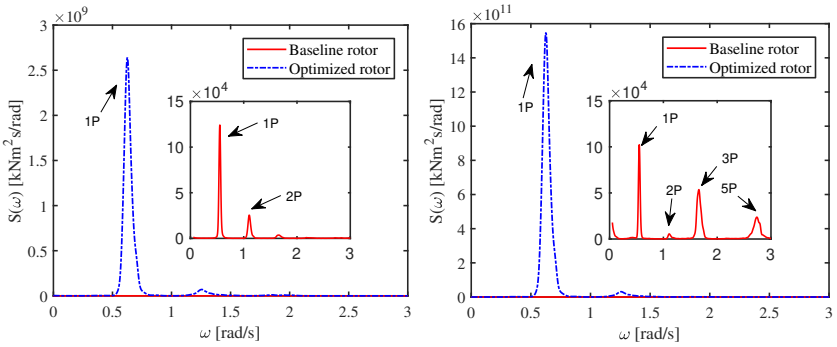

(a) Flapwise bending moment (b) Edgewise bending moment

Figure 16: Power spectra of (a) flapwise bending moment and (b) edgewise bending moment at the mid of the blade of the floating VAWTs with the baseline and optimized rotors under LC3.

5.6. Characteristics of mooring line tensions

For both the floating VAWTs with the baseline rotor and with the optimized rotor, the mooring line 2 is aligned with the wind and wave direction, and hence it carries the largest mooring line loads among the three mooring lines. The tension in mooring line 2 is thus investigated in this section.

An example of time history of tension in mooring line 2 under LC7 is demonstrated in Fig. 17. It can be easily identified that the floating VAWT with the

optimized rotor has smaller tension in mooring line 2. Fig. 18 summarizes and presents the mean values and standard deviations of the tension in mooring line 2 for both floating VAWTs under turbulent wind and irregular waves. It can be found that for the wind speed above 14 m/s, the mean tension in mooring line 2 for the floating VAWT with the optimized rotor is relatively smaller than that with the baseline rotor. Regarding the standard deviation of the tension in mooring line 2, the value is about $\frac{1}{10}$ of the mean value, and the floating VAWT with the optimized rotor gives slightly larger value for the wind speed above 12 m/s.

Power spectral analyses are also carried out for the tension in mooring line 2, as shown in Fig. 19. In general, the tension in mooring line 2 is mainly dominated by low frequency responses, especially the surge resonant responses, due to turbulent winds. A small 2P response is observed for both floating VAWTs, and at high wind speed, the floating VAWT with the baseline rotor also presents a small resonant response at about 1.68 rad/s.

6. Conclusions

This study deals with the evaluation of performance enhancement of a semi-submersible type floating VAWT with an optimized rotor. The optimized rotor was developed in the DeepWind project, which was improved based on a baseline rotor. Both the baseline and optimized rotors are Darrieus type VAWTs, and

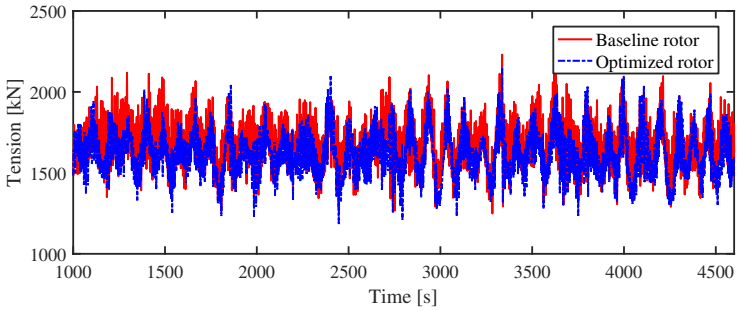

Figure 17: Time history of tension in mooring line 2 of the floating VAWTs with the baseline and optimized rotors under LC7.

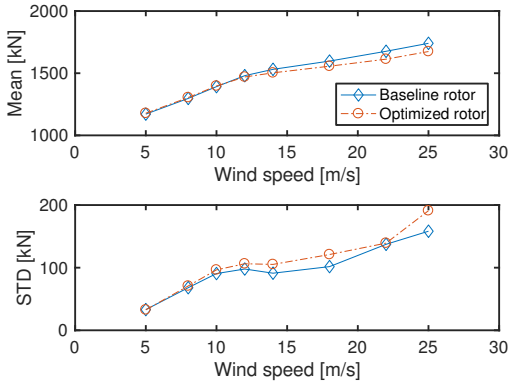

Figure 18: Mean values and standard deviations of tension in mooring line 2 of the floating VAWTs with the baseline and optimized rotors under turbulent wind and irregular waves.

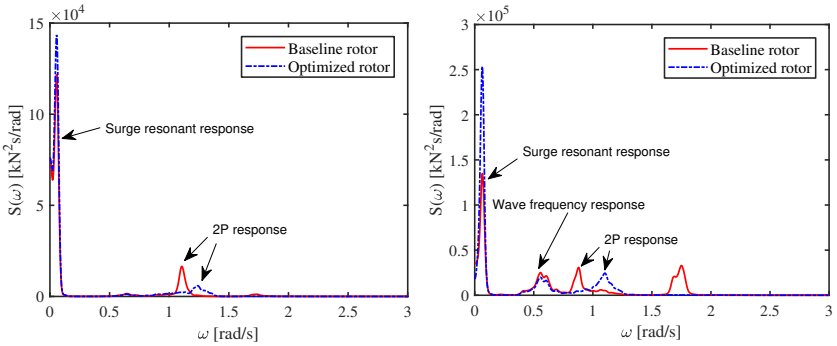

(a) under LC3 (b) under LC7

Figure 19: Power spectra of tension in mooring line 2 of the floating VAWTs with the baseline and optimized rotors under LC3 and LC7.

are adapted to a semi-submersible platform to achieve two floating VAWTs in this study. The performance enhancement of the floating VAWT with the optimized rotor is thus assessed mainly by comparison with the floating VAWT with the baseline rotor, considering the power production, aerodynamic loads, platform motions, and structural responses.

The assessment is based on time domain numerical simulations, in which a state-of-the-art fully coupled aero-hydro-servo-elastic simulation tool is used. Two controllers are specially designed and implemented for these two rotors.

They are capable of keeping the mean power production between the baseline and optimized rotors fairly close above the rated wind speed. A series of turbulent wind and irregular wave load cases are then simulated to achieve the dynamic responses of these two floating VAWTs.

The floating VAWT with the optimized rotor has better power performance than that with the baseline rotor. At the site considered, the annual power production of the optimized rotor is improved by 11.3%, which is approximately the same as an identical floater supporting the NREL 5MW horizontal axis wind turbine. Despite its better power performance, the aerodynamic loads on the optimized rotor is reduced compared to those of the baseline rotor, especially above the rated wind speed. Consequently, the global platform motions of the floating VAWT with the optimized rotor are generally smaller, except for the standard deviation of surge motion. The tower base bending moments of the floating VAWT with the optimized rotor are greatly reduced, due to much smaller 2P responses. The mean tension in mooring lines of the floating VAWT with the optimized is also decreased, despite a small increase in the standard deviation at high wind speeds.

Due to adjustments with respect to rotor geometry and blade materials, the blade load distributions of the optimized rotor differs significantly from those of the baseline rotor. The standard deviation of the flapwise and edgewise bending moments of the optimized rotor are greatly increased. Though the composite materials used for the blades have excellent anti-fatigue performance, the fatigue within the blades of the optimized rotor can still be an issue and should be noticed for the floating VAWT with the optimized rotor.

As a whole, the floating VAWT with the optimized rotor greatly improves the performances with respect to the power production, the global platform motions, the mooring line tensions, and the tower base bending moments as compared with the floating VAWT with the baseline rotor. However, the fatigue damage within the blade is not mitigated and should be carefully considered during the optimization of blades for VAWTs in the future.

Acknowledgements

The first author appreciates the support from State Key Laboratory of Hydraulic Engineering Simulation and Safety (HESS-1710), Tianjin University, China.

References

[1] Karimirad M, Moan T. Wave-and wind-induced dynamic response of a spar-type offshore wind turbine. Journal of waterway, port, coastal, and ocean engineering 2011;138(1):9–20.

[2] Kvittem MI, Bachynski EE, Moan T. Effects of hydrodynamic modelling in fully coupled simulations of a semi-submersible wind turbine. Energy Procedia 2012;24:351–62.

[3] Bachynski EE, Moan T. Design considerations for tension leg platform wind turbines. Marine Structures 2012;29(1):89–114.

[4] Paquette JA, Barone MF. Innovative offshore vertical-axis wind turbine rotor project. Tech. Rep.; Sandia National Laboratories (SNL-NM), Albuquerque, NM (United States); 2012.

[5] Wang K, Moan T, Hansen MOL. Stochastic dynamic response analysis of a floating vertical-axis wind turbine with a semi-submersible floater. Wind Energy 2016;19(10):1853–70.

[6] Dabiri JO. Potential order-of-magnitude enhancement of wind farm power density via counter-rotating vertical-axis wind turbine arrays. Journal of Renewable and Sustainable Energy 2011;3(4):043104.

[7] Paulsen US, Vita L, Madsen HA, Hattel J, Ritchie E, Leban KM, et al. 1st Deepwind 5MW baseline design. Energy Procedia 2012;24:27–35.

[8] Paulsen US, Madsen HA, Hattel JH, Baran I, Nielsen PH. Design optimization of a 5MW floating offshore vertical-axis wind turbine. Energy Procedia 2013;35:22–32.

[9] Cahay M, Luquiau E, Smadja C, Silvert F. Use of a vertical wind turbine in an offshore floating wind farm. In: Offshore technology conference. Offshore Technology Conference; 2011,.

[10] Cheng Z, Zhang P. Characteristic aerodynamic loads and load effects on the dynamics of a floating vertical axis wind turbine. Transactions of Tianjin University 2017;23(6):555–61.

[11] Wang K, Luan C, Moan T, Hansen MOL. Comparative study of a FVAWT and a FHAWT with a semi-submersible floater. In: Proceedings of the 24th International Ocean and Polar Engineering Conference. Busan, South Korea; 2014,.

[12] Cheng Z, Wang K, Gao Z, Moan T. A comparative study on dynamic responses of spar-type floating horizontal and vertical axis wind turbines. Wind Energy 2017;20(2):305–23.

[13] Cheng Z, Madsen HA, Chai W, Gao Z, Moan T. A comparison of extreme structural responses and fatigue damage of semi-submersible type floating horizontal and vertical axis wind turbines. Renewable Energy 2017;108:207–19.

[14] Cheng Z, Wang K, Gao Z, Moan T. Dynamic response analysis of three floating wind turbine concepts with a two-bladed darrieus rotor. Journal of Ocean and Wind Energy 2015;2:213–22.

[15] Cheng Z, Gao Z, Madsen HA, Moan T. Effect of the number of blades on the dynamics of floating straight-bladed vertical axis wind turbines. Renewable Energy 2017;101:1285–98.

[16] Vita L, Schmidt Paulsen U, Friis Pedersen T, Aagaard Madsen H, Rasmussen F. A novel floating offshore wind turbine concept. In: 2009 European Wind Energy Conference and Exhibition. 2009,.

[17] Verelst DR, Aagaard Madsen H, Kragh KA, Belloni F. Detailed load analysis of the baseline 5MW Deepwind concept. Tech. Rep.; DTU Wind Energy; 2014.

[18] Ishie J, Wang K, Ong MC. Structural dynamic analysis of semi-submersible floating vertical axis wind turbines. Energies 2016;9(12):1047.

[19] Wang K, Moan T, Hansen MOL. A method for modeling of floating vertical axis wind turbine. In: Proceedings of the ASME 32rd International Conference on Ocean, Offshore and Arctic Engineering. Nantes, France; 2013,.

[20] Paulsen US, Borg M, Madsen HA, Pedersen TF, Hattel J, Ritchie E, et al. Outcomes of the deepwind conceptual design. Energy Procedia 2015;80:329–41.

[21] Robertson A, Jonkman J, Masciola M, Song H, Goupee A, Coulling A, et al. Definition of the semi-submersible floating system for phase II of OC4. Report; 2012.

[22] Jonkman JM, Butterfield S, Musial W, Scott G. Definition of a 5-mw reference wind turbine for offshore system development. Tech. Rep. NREL/TP-500-38060; NREL, Golden, CO, USA; 2009.

[23] Cheng Z, Madsen HA, Gao Z, Moan T. A fully coupled method for numerical modeling and dynamic analysis of floating vertical axis wind turbines. Renewable Energy 2017;107:604–19.

[24] MARINTEK . Simo-theory manual version 4.0. 2012.

[25] MARINTEK . Riflex theory manual, version 4.0. 2012.

[26] Faltinsen OM. Sea loads on ships and offshore structures. Cambridge, UK: Cambridge University Press; 1995.

[27] Cheng Z, Madsen HA, Gao Z, Moan T. Aerodynamic modeling of offshore vertical axis wind turbines using the actuator cylinder method. Energy Procedia 2016;94:531 –43.

[28] Madsen HA. The Actuator Cylinder: A flow model for vertical axis wind turbines. Institute of Industrial Constructions and Energy Technology, Aalborg University Centre; 1982.

[29] Ferreira CS, Madsen HA, Barone M, Roscher B, Deglaire P, Arduin I. Comparison of aerodynamic models for vertical axis wind turbines. Journal of Physics: Conference Series 2014;524(1):012125.

[30] Ishie J. Structural dynamic analysis of semi-submersible floating vertical axis wind turbines. Master Thesis, University of Stavanger; 2016.

[31] Vita L. Offshore vertical axis wind turbine with floating and rotating foundation. Ph.D. thesis; Technical University of Denmark (DTU); 2011.

[32] Jonkman BJ. Turbsim user's guide: Version 1.50. 2009.

[33] IEC . International standard 61400-1, wind turbines, part 1: Design requirements. 2005.

[34] Johannessen K, Meling TS, Haver S. Joint distribution for wind and waves in the northern north sea. International Journal of Offshore and Polar Engineering 2002;12(1).